

# Effect of Tensile Loading and Temperature on the Hydrogen Solubility of Steels at High Gas Pressure

Andreas Karl Drexler,\* Florian Konert, Jonathan Nietzke, Emir Hodžić, Sergio Pastore, Josef Domitner, Michael Rhode, Christof Sommitsch, and Thomas Böllinghaus

The hydrogen solubility in ferritic and martensitic steels is affected by hydrostatic stress, pressure, and temperature. In general, compressive stresses decrease but tensile stresses increase the hydrogen solubility. This important aspect must be considered when qualifying materials for high-pressure hydrogen applications (e.g., for pipelines or tanks) by using autoclave systems. In this work, a pressure equivalent for compensating the effect of compressive stresses on the hydrogen solubility inside of closed autoclaves is proposed to achieve solubilities that are equivalent to those in pipelines and tanks subjected to tensile stresses. Moreover, it is shown that the temperature effect becomes critical at low temperatures (e.g., under cryogenic conditions for storing liquid hydrogen). Trapping of hydrogen in the microstructure can increase the hydrogen solubility with decreasing temperature, having a solubility minimum at about room temperature. To demonstrate this effect, the generalized law of the hydrogen solubility is parameterized for different steels using measured contents of gaseous hydrogen. The constant parameter sets are verified and critically discussed with respect to the high-pressure hydrogen experiments.

hydrogen embrittlement, which can reduce the lifetime of steel components by accelerating crack growth and fracture.<sup>[5–7]</sup> A mechanistic lifetime assessment is very difficult, as potential mechanisms of hydrogen embrittlement are not fully understood and thus extensively discussed.<sup>[8,9]</sup> Therefore, the qualification of structural materials with respect to their resistivity against hydrogen embrittlement mainly relies on experimental testing and standards.<sup>[10,11]</sup> Autoclave systems for testing and qualifying steels that are used in high-pressure applications of gaseous hydrogen are very common.<sup>[6,12–15]</sup> Two different setups are widely used: 1) closed autoclaves that do not allow for any manipulation of the samples during testing, and 2) autoclaves with protruding sample holders for quasi-static testing or fatigue testing under high-pressure hydrogen


## 1. Introduction

The transition toward “green” energy<sup>[1–3]</sup> needs structural materials for transmission and storage of high-pressured hydrogen gas. In particular, gas tanks or pipelines made of steel are of utmost interest for the distribution of gaseous hydrogen, because their production is environment-friendly and comparatively cheap, they are available in large quantities, and they possess high recyclability.<sup>[4]</sup> However, hydrogen absorption of ferritic and martensitic steels raises major concerns with regard to

atmosphere. Current guidelines, such as ASME B31.12<sup>[16]</sup> and DVGW G 464 (M),<sup>[17]</sup> and standards, like ISO 11114-4,<sup>[18]</sup> describe the mechanical testing and evaluation procedures in detail, but they are quite unspecific regarding the definition of the required hydrogen pressure that should be applied. The internal gas pressure in tanks or pipelines induces tensile hydrostatic stresses in the material, while the gas pressure applied inside of autoclave systems induces compressive hydrostatic stresses. Tensile stresses increase the hydrogen solubility, while compressive stresses lead to the opposite effect. This would cause differences in the hydrogen solubility of materials in laboratory conditions (autoclave) and under service conditions. Since the hydrogen solubility is sensitive to mechanical stresses,<sup>[19]</sup> the autoclave setup and the sample geometry<sup>[20]</sup> can both influence the results of embrittlement testing. Another issue is the missing information about the hydrogen solubility of ferritic and martensitic steels at low temperatures. According to the classical law of Sieverts,<sup>[21]</sup> the hydrogen solubility decreases with temperature. A review of measured solution enthalpies of ferritic and martensitic steels revealed an endothermic value around 27 kJ mol<sup>-1</sup>.<sup>[19]</sup> In other words, the temperature dependency of the solubility of hydrogen in iron and steels causes a negative slope in the Arrhenius graph. This is in contrast to the hydrogen solubility of other metals, such as titanium or vanadium, which have a much higher affinity to hydrogen. An overview of the gaseous hydrogen solubility of different pure metals is provided in ref. [22]. In the past, measurements used for parameterizing

A. K. Drexler, E. Hodžić, S. Pastore, J. Domitner, C. Sommitsch  
Institute of Materials Science, Joining and Forming  
Research Group of Lightweight and Forming Technologies  
Graz University of Technology  
Inffeldgasse 11/I, 8010 Graz, Austria  
E-mail: andreas.drexler@gmx.net

F. Konert, J. Nietzke, M. Rhode, T. Böllinghaus  
Department 9 - Component Safety  
Bundesanstalt für Materialforschung und -prüfung (BAM)  
Unter den Eichen, 87, 12205 Berlin, Germany

 The ORCID identification number(s) for the author(s) of this article can be found under <https://doi.org/10.1002/srin.202300493>.

© 2023 The Authors. Steel Research International published by Wiley-VCH GmbH. This is an open access article under the terms of the Creative Commons Attribution License, which permits use, distribution and reproduction in any medium, provided the original work is properly cited.

DOI: 10.1002/srin.202300493

Sieverts' law mainly rely on permeation setups at high temperatures and low pressures;<sup>[23]</sup> however, many applications for steel are designed for temperatures far below 100 °C and for high hydrogen pressures up to 1000 bar. Under such conditions, trapping of hydrogen in the microstructure can increase the actual hydrogen solubility beyond the solubility predicted by Sieverts' law.<sup>[19]</sup> Therefore, this work studies the influence of temperature and tensile stresses on the hydrogen solubility of ferritic and martensitic steels in gaseous hydrogen. The thermodynamic theory of the solubility of gaseous hydrogen is summarized by considering hydrogen trapping in the microstructure and the behavior of real gas. Solubilities of gaseous hydrogen are measured to parameterize and to verify the generalized solubility law. Solubility curves are calculated as function of temperature and pressure. Finally, the parameterized solubility law is used to derive a pressure equivalent that compensates the hydrogen solubility in closed autoclaves, which is tendentially lower than the solubility under industrial applications.

## 2. Thermodynamic Theory

The hydrogen solubility in steels,  $s$ , is the maximum total hydrogen concentration that is dissolved under specific external mechanical loading  $\sigma$ , outer partial pressure  $p_{H_2}$ , and temperature  $T$ . According to the theory of McNabb and Foster,<sup>[24]</sup>  $s$  comprises the lattice hydrogen concentration  $c_L$  and the trapped hydrogen concentration  $c_T$

$$s = c_L + c_T \quad (1)$$

An example of experimental observations of trapped hydrogen atoms in ferritic and martensitic steels is given by Chen et al.<sup>[25,26]</sup> Lattice hydrogen diffuses through the crystal by jumping between neighboring interstitial lattice sites and by exchange with the outer pressurized gas. In accordance with the work of Krom and Bakker,<sup>[27]</sup> hydrogen transport along the grain boundaries and dislocations is not considered as important for ferritic or martensitic steels, which was also experimentally verified for Armco iron by Siegl et al.<sup>[28,29]</sup> In thermodynamic equilibrium, the chemical potentials of hydrogen in the gas phase and of hydrogen dissolved in the interstitial lattice must be equal  $\frac{1}{2}\mu_{H_2} = \mu_L$ . The chemical potential of gaseous hydrogen is

$$\mu_{H_2} = \mu_{H_2,0} + RT \ln(f) \quad (2)$$

and the generalized chemical potential of lattice hydrogen is

$$\mu_L = \mu_0 + RT \ln(\gamma_L) - \sigma_H V_H \quad (3)$$

Inserting Equation (2) and (3) into the standard equilibrium condition gives the gives Sieverts' law,<sup>[21,30]</sup> which allows to calculate  $c_L$  as function of pressure, temperature, and the hydrostatic stress<sup>[31,32]</sup>

$$c_L = K_0 \sqrt{f} \exp\left(-\frac{\Delta H_s - \sigma_H V_H}{RT}\right) \quad (4)$$

$K_0$  is a constant,  $\Delta H_s$  is the solution enthalpy,  $V_H$  is the partial molar volume of hydrogen,  $R$  is the universal gas constant,  $T$  is the temperature, and  $\gamma_L$  is the lattice site fraction.  $K_0$  considers

the attempt frequency and the entropy,<sup>[33,34]</sup> and  $\Delta H_s$  represents the energy difference between hydrogen molecules in vacuum and hydrogen atoms in the lattice. Values larger than zero represent endothermic absorption reactions. The hydrostatic stress is defined as  $\sigma_H = \frac{1}{3} \text{tr}(\sigma_{ij})$ , where  $\text{tr}(\sigma_{ij})$  is the trace of the stress tensor  $\sigma_{ij}$ . The fugacity  $f$  is given as

$$f = p_{H_2} \exp\left(\frac{p_{H_2} b}{RT}\right) \quad (5)$$

where  $b$  is the van der Waals constant,<sup>[35]</sup> which describes the difference between the behaviors of real hydrogen gas and ideal gas at low temperature and high pressure. Trapping sites increase the solubility of hydrogen and decrease the diffusivity.<sup>[27,36–41]</sup> Based on their binding energy  $E_b$ , they are classified as shallow sites ( $E_b < 60 \text{ kJ mol}^{-1}$ ) or deep sites ( $E_b \geq 60 \text{ kJ mol}^{-1}$ ). For example, dislocations are shallow sites,<sup>[29,42]</sup> while vacancies are deep sites.<sup>[42,43]</sup> Drexler et al.<sup>[20,44]</sup> showed numerically that trapping sites with  $E_b \geq 60 \text{ kJ mol}^{-1}$  strongly retard chemical diffusion. Hence, hydrogen desorption from deep trapping sites behaves quasi-irreversible at room temperature. According to Svoboda and Fischer,<sup>[45]</sup> the chemical potential of trapped hydrogen can be written as

$$\mu_T = \mu_0 + RT \ln\left(\frac{\gamma_T}{1 - \gamma_T}\right) - E_b \quad (6)$$

$\gamma_T$  is the site fraction of trapped hydrogen. The standard equilibrium condition  $\mu_L = \mu_T$  in conjunction with Equation (3) and (6) provides the equilibrium trap concentration  $c_T$  depending on the lattice concentration  $c_L$ .<sup>[45,46]</sup>

$$c_T = \frac{c_L N_T}{N_L \left(K + \frac{c_L}{N_L} (1 - K)\right)} \quad (7)$$

where  $K = \exp(-E_b/RT)$  is the equilibrium constant,  $N_T$  is the trap density, and  $N_L$  is the lattice site density.  $N_T$  and  $E_b$  characterize the defect density of the microstructure and the type of defect, respectively. In the present work, the effect of pure (100 vol%) hydrogen gas is studied and thus the total pressure  $p$  equals the hydrogen partial pressure  $p_{H_2}$ . The influence of mechanical loading on the hydrogen solubility is studied for the two conditions illustrated in **Figure 1**: a) samples in closed autoclaves experience a hydrostatic stress which is equal to the negative gas pressure,  $\sigma_H = -p_{H_2}$ ; b) if the gas pressure  $p$  is superposed with the axial tensile stress  $\sigma_1$ , the hydrostatic stress is defined as  $\sigma_H = \frac{\sigma_1}{3} - \frac{2}{3} p_{H_2}$ . Only elastic straining is considered in the present work. Plastic straining would increase the trap concentration by hydrogen-enhanced strain induced defect formation.<sup>[43,47]</sup> Normally, the axial tensile loading  $\sigma_1$  is controlled by the outer tensile machine. In the case of a given sample displacement, the high gas pressure  $p_{H_2}$  causes additional transverse strain and thus affects the tensile stress. If no displacement or loading is applied, it is assumed that the sample can freely move in axial direction.

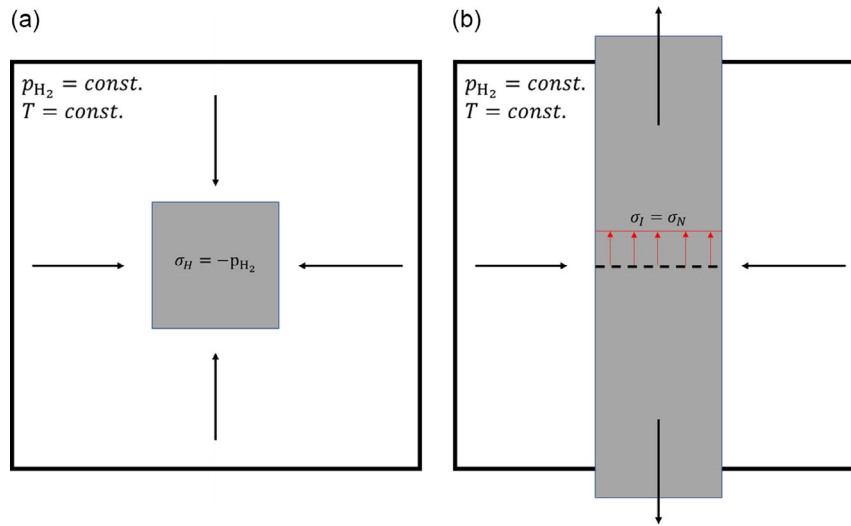


**Figure 1.** Schematic illustrations of a) testing of a sample in a closed pressurized autoclave and b) tensile testing of a sample protruding the pressurized autoclave.

### 3. Experimental Section

#### 3.1. Measurement of Gaseous Hydrogen

Samples of 34CrMo4 and three industrial dual-phase (DP) steels were machined for gaseous hydrogen charging and subsequent thermal desorption analysis (TDA). The chemical compositions are given in Table 1. The 34CrMo4 steels possessed a ferritic microstructure. Details of the ferritic–martensitic microstructure of the DP steels are given in ref. [48]. The sample size of the 34CrMo4 steels was cubic with an edge length of 4.5 mm, while the DP steel samples had the dimensions 100 × 10 × 1.2 mm. Before the samples were placed inside the autoclave for charging in gaseous hydrogen, the surfaces were ground, polished, and rinsed with acetone. To reduce the remaining oxygen in the autoclave, it was purged several times with pure nitrogen gas. High-pressure hydrogen gas was applied at elevated temperatures with a charging time of minimum of 3 weeks. Pressure, temperature, and corresponding hydrogen solubility are summarized in Table A1. After hydrogen charging, the samples were removed from the autoclave and immediately stored in liquid nitrogen to prevent desorption losses during transportation. The surface quality did not change during gaseous hydrogen charging. Directly before TDA, the samples were thawed in acetone and dried using compressed nitrogen gas. A Bruker Galileo G8 carrier gas hot extraction (CGHE) analyzer was used for measuring the hydrogen content isothermal at 400 °C<sup>[49,50]</sup> using an infrared furnace and an ESD 100a mass spectrometer from InProcess

**Table 1.** Chemical composition of investigated materials.

Materials	C	Cr + Mo	Mn	P	S	Si	Ti+Nb	B	Cu
32CrMo4	0.28	0.94 + 017	0.72	0.007	0.002	0.22	–	–	–
DP600	<0.15	<1.40	<2.50	<0.050	<0.010	<0.80	<0.15	<0.005	<0.20
DP800	<0.18	<1.40	<2.50	<0.050	<0.010	<0.80	<0.15	<0.005	<0.20
DP1000	<0.20	<1.40	<2.50	<0.050	<0.010	<0.80	<0.15	<0.005	<0.20

Instruments. Further details on the applied CGHE procedure can be found in ref. [37].

#### 3.2. Inverse Parameterization Routine

For inverse determination of the trapping parameters  $E_b$  and  $N_T$ , the measured hydrogen contents were fitted as function of the pressure and the temperature. For that purpose, gaseous hydrogen contents of different low alloyed steels with a ferritic or martensitic matrix were measured and collected from literature.<sup>[13,19,48,51–53]</sup> A summary of the literature data is given in a tabular form in Appendix. All measurements were performed using the TDA method after high-pressure hydrogen charging of samples in closed autoclave systems. To improve the comparability of the data, the yield strength and tensile strength were also

**Table 2.** Parameterization of Equation (4) and (5) to calculate the lattice hydrogen concentration.

Description	Symbol	Value	References
Constant	$K_0$	$1.81 \times 10^{-7} \text{ mol mm}^{-3} \text{ MPa}^{-0.5}$	[23]
Solution enthalpy	$\Delta H_s$	$27 \text{ kJ mol}^{-1}$	[63]
Partial molar volume of hydrogen	$V_H$	$2 \times 10^3 \text{ mm}^3 \text{ mol}^{-1}$	[64]
Density of interstitial lattice sites	$N_L$	$2.04 \times 10^{-4} \text{ mol mm}^{-3}$	[45]
Van der Waals constant	$b$	$0.1584 \text{ mm}^3 \text{ mol}^{-1}$	[35]

included in Table A1 (if available). The material designations were adopted from the original reference. An optimization routine was developed using Python scripting. This optimizer was based on the algorithm of Nelder and Mead<sup>[54]</sup> to minimize the residuum  $R^2$ , which is defined as

$$R^2 = \frac{\sum_{i=1,N} (c_i - s_i)^2}{\sum_{i=1,N} (c_i - \bar{c})^2} \quad (8)$$

**Table 3.** Inversely fitted trapping parameters based on measured hydrogen contents.

Material	Binding energy [ $E_b$ , kJ mol <sup>-1</sup> ]	Trap density [ $N_T$ , mol mol <sup>-3</sup> ]
Iron	42.21	$2.32 \times 10^{-9}$
L80	19.42	$1.05 \times 10^{-5}$
L450	17.70	$1.65 \times 10^{-5}$
34CrMo4	39.97	$2.13 \times 10^{-8}$
42CrMo4	33.55	$3.56 \times 10^{-8}$
P110	19.1	$1.39 \times 10^{-5}$
DP600	22.06	$3.22 \times 10^{-6}$
DP800	21.77	$2.79 \times 10^{-6}$
DP1000	21.50	$4.60 \times 10^{-6}$

where  $\bar{c}$  is the arithmetic mean of the measured hydrogen contents;  $c_i$  and  $s_i$  are the solubilities calculated using Equation (1).

## 4. Results and Discussion

### 4.1. Solubility Curves

The temperature dependency of the hydrogen solubility is influenced by the number of trapping sites in the microstructure and by the solution enthalpy of the interstitial lattice sites. The trap concentration decreases and the lattice concentration increases with increasing thermal activation. These opposite dependencies can cause a minimum of the hydrogen solubility at approximately room temperature, which depends on the trapping parameters  $E_b$  and  $N_T$ .<sup>[19]</sup> This minimum is not considered in the classical Sieverts' law,<sup>[21]</sup> which assumes an exponential decrease of the gas solubility with decreasing temperature. Hence, extrapolation to lower temperatures using Sieverts' law would significantly underestimate the solubility of gaseous hydrogen. The complex temperature dependency must be considered for the appropriate measurement of the hydrogen solubility. This is of particular importance for qualifying gas tanks or pipelines at temperatures down to  $-40^\circ\text{C}$ .<sup>[55]</sup>

To verify the theoretical assumptions, the measurement of hydrogen contents at temperatures below room temperature is

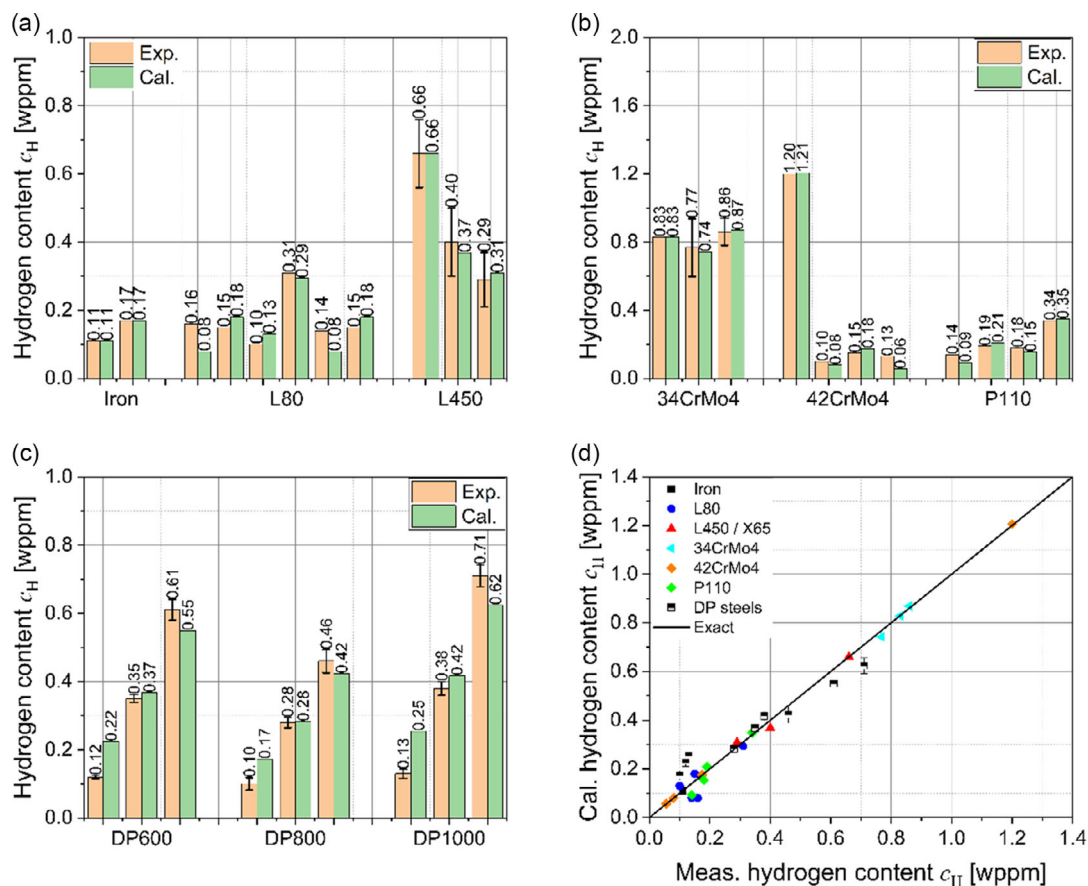


**Figure 2.** Verification of the parameter settings by comparing the calculated total hydrogen solubility with measured hydrogen contents for different materials:<sup>[13,19,51–53]</sup> a–c) bar diagrams and d) predicted versus measured diagram.

of utmost importance. However, collecting measured gaseous hydrogen contents for different ferritic and martensitic steels demonstrates that most gaseous charging is performed in literature between room temperature and 100 °C. Moreover, the increased diffusivity at higher temperatures makes measuring the solubility of gaseous hydrogen in autoclave systems difficult. Releasing the pressure and cooling the autoclave needs several minutes. During this time, the hydrogen content in the samples may decrease, which would not represent the initial charging parameters. Even though this effect is less significant at temperatures below room temperature, the general time for charging steel with gaseous hydrogen increases since the diffusivity decreases with decreasing temperature.

For extrapolating and interpolating the solubility of gaseous hydrogen by using Equation (1), (4), (5), and (7), seven constant parameters must be determined for each steel. Five of these seven parameters are virtually independent from the microstructure of many low alloyed steels with ferritic or martensitic microstructures;<sup>[19]</sup> however, the trapping parameters  $E_b$  and  $N_T$  are sensitive to the composition and to the thermomechanical treatment of the steel. As summarized in **Table 2**, the independent parameters of pure ferritic iron were used in this work.  $K_0$  and  $\Delta H_s$  must be determined at the high-temperature regime, where hydrogen trapping at microstructural defects is fully thermally activated. Reliable measurement setups are permeation cells with gaseous charging and in situ measurements, e.g., as presented in

ref. [56]. Because of the time delay during opening, autoclaves cannot be used for determining those parameters.

Furthermore, the applied gas pressure inside of the autoclave decreases the solution enthalpy, which induces compressive hydrostatic stresses inside the sample. Hence, measured and ab initio calculated values of the partial molar volume of hydrogen in ferritic iron,  $V_H$ , were considered.<sup>[19]</sup> According to Hirth,<sup>[57]</sup>  $V_H$  is quite similar in each of the investigated metals. The density of interstitial lattice  $N_L$  sites is given by Svoboda and Fischer.<sup>[45]</sup>

From a thermodynamic point of view, defects with equal binding energies contribute to the same trapping sites and cannot be distinguished by TDA. The trapping parameters summarized in **Table 3** were independently fitted for each material using the measured hydrogen contents. Due to limited number of measured hydrogen contents for each material and to avoid over-parameterization, only a single-trap approach was considered in the present work. Nevertheless, Equation (1) can easily be extended to take multiple trapping sites into account, as described in refs. [41,58,59]. According to the binding energies, the materials contain shallow trapping sites with trap densities from  $2.32 \times 10^{-9} \text{ mol mm}^{-3}$  for pure iron to  $1.65 \times 10^{-5} \text{ mol mm}^{-3}$  for L450 steel. In addition to the binding energy, the trap density has a significant influence on the trapping capacity.

**Figure 2** verifies the parameter sets that describe the solubility of hydrogen in the investigated materials by comparing measured and calculated gaseous hydrogen contents. The set of seven

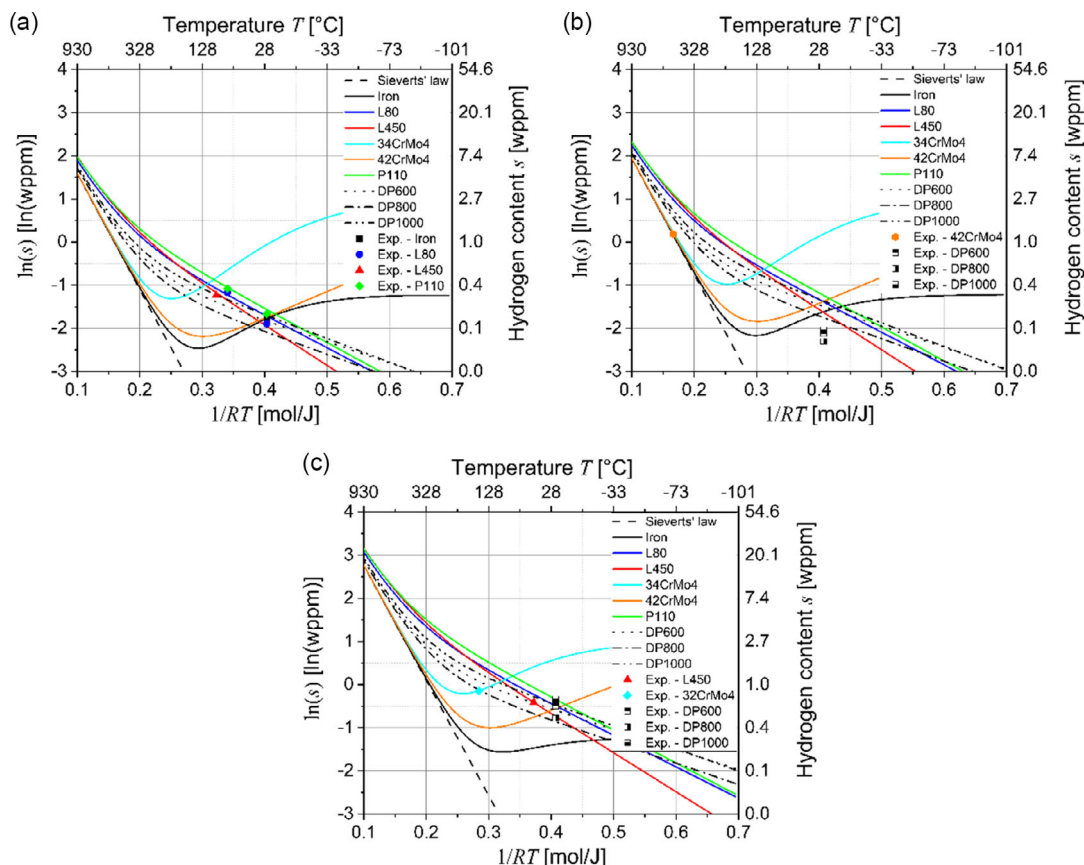


**Figure 3.** Solubility of gaseous hydrogen at a) 100 bar, b) 200 bar, and c) 1000 bar as function of the temperature.



parameters enables predicting the content of gaseous hydrogen absorbed by a given material for wide pressure and temperature ranges. As demonstrated in Figure 2d, the hydrogen contents predicted by using the solubility equations and the parameter sets only differ by about  $\pm 0.1$  wppm from the hydrogen contents measured using TDA and found in the literature.

Figure 3 shows the calculated evolution of the hydrogen solubility as function of the temperature at the gas pressures of a) 100, b) 200, and c) 1000 bar. Measured hydrogen contents are added as symbols. The parameter sets were constant for each material and independent from temperature and pressure. Due to the thermal activation of trapping sites, the solubility of iron and CrMo-steels has a minimum at about 100 °C, causing an increase of the hydrogen uptake with decreasing temperatures. The solubility of the other steels decreases with decreasing temperature.<sup>[21,23,60]</sup> However, as shown in Figure 3, Sievert's law generally underestimates the solubility of gaseous hydrogen at temperatures below 200 °C. Thus, extrapolating hydrogen contents measured in the temperature regime between room temperature and 100 °C to either higher or lower values leads to an incorrect prediction of the hydrogen solubility.

#### 4.2. Pressure Equivalent for Testing in Autoclave Systems

As shown in Figure 4 for room temperature, the hydrogen solubility generally increases with increasing hydrogen pressure. Since the sample is exposed to compressive hydrostatic stress inside of closed autoclaves, the hydrogen solubility is always lowest compared to applications with tensile hydrostatic stresses.<sup>[19]</sup> Superposing compressive stresses with tensile stresses, e.g., by using autoclaves with protruding sample holders, increases the hydrogen solubility with respect to the reference measurements using just closed autoclaves. As shown in Figure 4, this difference in the solubility depends on the material, and it can reach about 0.2 wppm at the gas pressure of 1000 bar.

The effect of tensile loading on the hydrogen solubility was strongest for the P110 steel and lowest for iron. Among the investigated materials, iron has the lowest trap density and, thus, the lowest capacity for hydrogen trapping. Trapping sites can increase the effect of tensile loading on the overall hydrogen solubility, which is due to the dependency of the equilibrium trap concentration from the lattice concentration. In other words, the effect of stresses on the hydrogen solubility can be decreased by developing steels with lower trapping capacity, e.g., by avoiding deep trapping at carbide interfaces.<sup>[61]</sup>

In many applications such as gas tanks or pipelines, the internal working pressure causes tensile stresses at the surface of the steel components.<sup>[19]</sup> As tensile stresses are identified to increase the hydrogen solubility, qualification tests in closed autoclaves should also be performed at higher gas pressures to establish equal conditions of hydrogen solubility. The required increase of the effective gas pressure inside of closed autoclaves to ensure conditions equal to real applications ("pressure equivalent") is marked with arrows in Figure 4.

Figure 5 shows that the pressure equivalent depends not only on the working pressure in the gas tanks or pipelines, but also on additional tensile loading in the component. However, the pressure equivalent seems to be virtually independent from the steel.

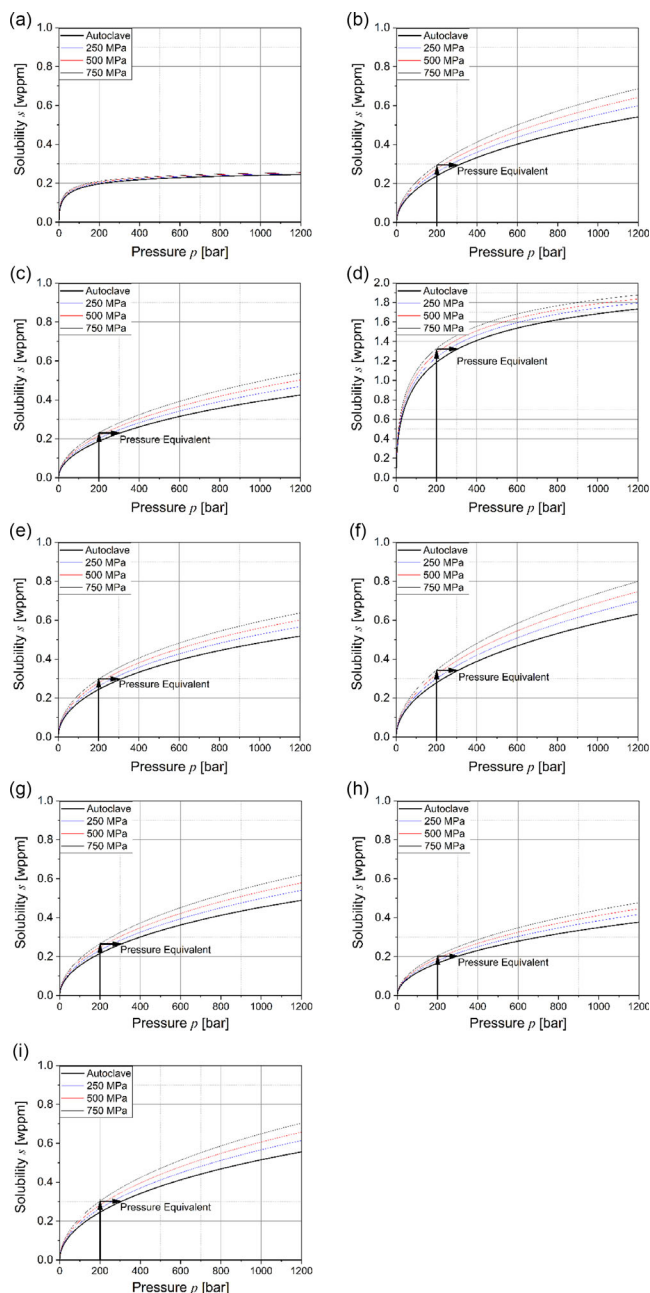


**Figure 4.** Influence of the tensile stress on the hydrogen solubility at room temperature: a) iron, b) L80, c) L450, d) 34CrMo4, e) 42CrMo4, f) P110, g) DP600, h) DP800, and i) DP1000.

A simple equation is proposed for calculating the pressure that must be applied in the closed autoclave,  $p_{au}$ , depending on the tensile stress  $\sigma_1$  and on the working pressure  $p$  inside of pipelines, gas tanks, etc.

$$p_{au} = (1 + k\sigma_1)p \quad (9)$$

with  $k = 8.6 \times 10^{-4} \text{ MPa}^{-1}$ . Thus, Equation (9) enables compensating the additional tensile loading in gas tanks or pipelines, or in material qualification tests using autoclave systems instead of

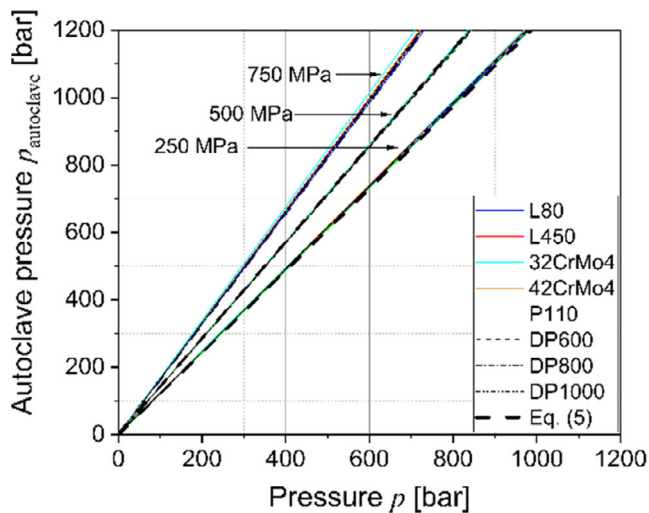


**Figure 5.** Equivalent pressure to compensate tensile stresses.

using just the working pressure. In future, steels have to be qualified for gaseous hydrogen applications always at pressures above the maximum operating pressure (MOP). For example, in the standard SAE J2579 for hydrogen vehicles,<sup>[62]</sup> slow strain rate tests or fatigue tests have to be performed using autoclave test rigs at an overpressure of 125%. Assuming an MOP of 700 bar in mobile applications, a minimum testing pressure of 875 bar is necessary. Furthermore, this standard request testing temperatures between  $-40$  and  $80$  °C. Understanding all the factors of influence on the hydrogen solubility and uptake, such as gas pressure, temperature, and mechanical stress, is a necessary precondition for designing suitable test rigs and performing reliable mechanical tests with respect to hydrogen embrittlement.

## 5. Summary and Conclusions

The solubility of gaseous hydrogen depends on the hydrostatic stress, the partial hydrogen pressure, the temperature, and

microstructure. A thermodynamic-based analytical model for predicting the increased hydrogen solubility (hydrogen uptake) with decreasing temperature was presented, which enables assessing the hydrogen embrittlement risk of storage applications (e.g., gas tanks or underground gas reservoirs) at low temperatures. To verify the analytical predictions, the results were compared with measured hydrogen contents for different steels of ferritic and martensitic microstructures. The generalized solubility law was parameterized for nine materials between room temperature and  $450$  °C and for pressures between  $20$  and  $1000$  bar. The accuracy of the analytical model was generally very good, and the difference to the measured hydrogen contents was less than  $\pm 0.1$  wppm. This enabled extrapolating the solubility of gaseous hydrogen to lower/higher temperature and pressure. The temperature dependency of the hydrogen solubility was identified as very complex. In particular, extrapolating the solubility to lower temperatures by using Sieverts' law can be considered as very critical with regard to the validity of the results, because Sieverts' law tends to underestimate the hydrogen uptake by orders of magnitude. Nevertheless, determining the solubility of gaseous hydrogen at temperatures below room temperature is of utmost importance, since lack of experimental data particularly exists in the cryogenic temperature regime. The qualification of steels for applications with pressurized gaseous hydrogen by using autoclave systems should always be performed at testing pressures above the nominal working pressure. However, the current guidelines and standards for specifying the necessary testing pressure are quite unprecise. The internal gas pressure causes tensile stresses in components such as gas tanks or pipelines, while samples inside of closed autoclaves are always exposed to compressive hydrostatic stresses. These stresses influence the solubility of hydrogen in the steels. A pressure equivalent for considering the working pressure and the tensile stresses was proposed to compensate the lower hydrogen solubility in autoclaves. This pressure equivalent was almost independent from the investigated steels.

## Appendix

**Table A1.** Summary of experimental data used in the present work to verify the parameter sets.

Material	$R_{p0.2}$ [MPa]	$R_m$ [MPa]	Pressure [bar]	Temperature [°C]	Measured hydrogen content [wppm]	References
34CrMo4	840	910	150	50	0.83	This work
34CrMo4	840	910	700	150	0.77	This work
34CrMo4	840	910	1000	150	0.86	This work
L450	–	–	100	100	0.29	This work
L450	–	–	1000	50	0.66	[19]
L450	–	–	200	80	0.4	[19]
P110	921	1015	20	25	0.14	[13]
P110	921	1015	100	25	0.19	[13]
P110	921	1015	20	80	0.18	[13]
P110	921	1015	100	80	0.34	[13]
42CrMo4	765	1014	20	25	0.1	[13]

Table A1. Continued.

Material	$R_{p0.2}$ [MPa]	$R_m$ [MPa]	Pressure [bar]	Temperature [°C]	Measured hydrogen content [wppm]	References
42CrMo4	765	1014	100	25	0.15	[13]
42CrMo4	765	1014	20	80	0.13	[13]
42CrMo4	765	1014	100	80	0.54	[13]
L80	607	721	20	25	0.16	[13]
L80	607	721	100	25	0.15	[13]
L80	607	721	20	80	0.1	[13]
L80	607	721	100	80	0.31	[13]
Armco iron	–	255	20	25	0.11	[51]
Armco iron	–	255	100	25	0.17	[51]
L80	>552	780	20	25	0.14	[51]
L80	>552	780	100	25	0.15	[51]
42CrMo4—700 °C	622	710	195	450	1.2	[53]
42CrMo4—650 °C	820	905	195	450	1.2	[53]
DP600	356	646	200	22	0.12	Hydrogen contents measured in this work; mechanical properties taken from ref. [65]
DP600	356	646	500	22	0.35	
DP600	356	646	1000	22	0.61	
DP800	520	826	200	22	0.1	
DP800	520	826	500	22	0.28	Hydrogen contents measured in this work; mechanical properties taken from ref. [65]
DP800	520	826	1000	22	0.46	
DP1000	733	1097	200	22	0.13	
DP1000	733	1097	500	22	0.38	Hydrogen contents measured in this work; mechanical properties taken from ref. [65]
DP1000	733	1097	1000	22	0.71	

## Acknowledgements

The authors thank Enrico Valverde Laks for providing the measured gaseous hydrogen contents of 34CrMo4 steels.

## Conflict of Interest

The authors declare no conflict of interest.

## Data Availability Statement

The data that support the findings of this study are available from the corresponding author upon reasonable request.

## Keywords

autoclaves, gaseous hydrogen, solubilities, steels, testings

Received: July 25, 2023  
Revised: September 17, 2023  
Published online:

- [1] European Commission, *Eur. Comm.* **2019**, 53, 24.  
[2] H. K. Pinegar, M. S. Moats, H. Y. Sohn, *Steel Res. Int.* **2011**, 82, 951.

- [3] K. Rechberger, A. Spanlang, A. Sasiain Conde, H. Wolfmeir, C. Harris, *Steel Res. Int.* **2020**, 91, 2000110.  
[4] N. E. Laadel, M. El Mansori, N. Kang, S. Marlin, Y. Boussant-Roux, *Int. J. Hydrogen Energy* **2022**, 47, 32707.  
[5] E. G. Ohaeri, W. Qin, J. Szpunar, *J. Alloys Compd.* **2021**, 857, 158240.  
[6] J. Ronevich, in *Proc. of the Fourth Int. Conf. on Metals & Hydrogen*, OCAS, Ghent, Belgium **2022**.  
[7] A. Massone, A. Manhard, A. Drexler, C. Posch, W. Ecker, V. Maier-Kiener, D. Kiener, *Materials* **2020**, 13, 4677.  
[8] S. Lynch, *Corros. Rev.* **2019**, 37, 377.  
[9] O. Barrera, D. Bombac, Y. Chen, T. D. Daff, E. Galindo-Nava, P. Gong, D. Haley, R. Horton, I. Katzarov, J. R. Kermod, C. Liverani, M. Stopher, F. Sweeney, *J. Mater. Sci.* **2018**, 53, 6251.  
[10] C. P. Looney, Z. M. Hagan, M. J. Connolly, P. E. Bradley, A. J. Slifka, R. L. Amaro, *Int. J. Fatigue* **2020**, 132, 105339.  
[11] H. Elsayed, A. Drexler, F. Warchomicka, I. Traxler, J. Domitner, M. Galler, R. Vallant, *J. Mater. Eng. Perform.* **2022**, 32, 5186.  
[12] A. Trautmann, G. Mori, W. Siegl, M. Truschner, J. Pfeiffer, M. Kapp, A. Keplinger, M. Oberndorfer, S. Bauer, *Berg- hüttenmänn. Monatsh.* **2019**, 165, 338.  
[13] A. Trautmann, G. Mori, M. Oberndorfer, S. Bauer, C. Holzer, C. Dittmann, *Materials* **2020**, 13, 3604.  
[14] L. Blanchard, L. Briottet, M. Bertin, A. Lriverain, O. Levasseur, in *Proc. of the Fourth Inter. Conf. on Metals & Hydrogen*, OCAS, Ghent, Belgium **2022**.  
[15] H. Matsunaga, in *Proc. of the Fourth Int. Conf. on Metals & Hydrogen*, OCAS, Ghent, Belgium **2022**.



- [16] ASME, B31.12-2019 Hydrogen Piping and Pipelines, ASME, New York, USA **2020**, B31.12-2, p. 280.
- [17] DVGW G 464 (M), Fracture-Mechanical Assessment Concept for Steel Pipelines with a Design Pressure of More than 16 Bar for the Transport of Hydrogen, DVGW, Bonn, Germany **2023**, G 464 (M), p. 20.
- [18] ISO, 11114-4:2017 Transportable Gas Cylinders – Compatibility of Cylinder and Valve Materials with Gas Contents - Part 4: Test Methods for Selecting Steels Resistant to Hydrogen Embrittlement, ISO, Geneva, Switzerland **2017**, p. 23.
- [19] A. Drexler, F. Konert, O. Sobol, M. Rhode, J. Domitner, C. Sommitsch, T. Böllinghaus, *Int. J. Hydrogen Energy* **2022**, *47*, 39639.
- [20] A. Drexler, J. Domitner, C. Sommitsch, in *Modeling of Hydrogen Diffusion in Slow Strain Rate (SSR) Testing of Notched Samples* (Eds: V. A. Polyanskiy, A. K. Belyaev) Vol. 143, Springer Nature, Switzerland AG **2021**.
- [21] A. Sieverts, W. Krumbhaar, *Berichte der Dtsch. Chem. Gesellschaft* **1910**, *43*, 893.
- [22] M. Nagumo, *Fundamentals of Hydrogen Embrittlement*; Springer Singapore, Singapore **2016**.
- [23] V. L. Gadgeel, D. L. Johnson, *J. Mater. Energy Syst.* **1979**, *1*, 32.
- [24] A. McNabb, P. K. Foster, *Trans. Met. Soc. AIME* **1963**, *227*, 618.
- [25] Y.-S. S. Chen, H. Lu, J. Liang, A. Rosenthal, H. Liu, G. Sneddon, I. McCarroll, Z. Zhao, W. Li, A. Guo, J. M. Cairney, *Science* **2020**, *367*, 171.
- [26] Y. E. Chen, R. Niu, P. Liu, P. Burr, J. Cairney, *Microsc. Microanal.* **2022**, *28*, 1618.
- [27] A. H. M. Krom, A. Bakker, *Metall. Mater. Trans. B* **2000**, *31*, 1475.
- [28] W. Siegl, W. Ecker, J. Klarner, G. Kloesch, G. Mori, A. Drexler, G. Winter, H. Schnideritsch, in *Proc. of the NACE – Int. Corrosion Conf. Series*, Vol. 2019, NACE International, Nashville, TN **2019**, pp. 1–12.
- [29] A. Drexler, W. Siegl, W. Ecker, M. Tkadletz, G. Klösch, H. Schnideritsch, G. Mori, J. Svoboda, F. D. Fischer, *Corros. Sci.* **2020**, *176*, 109017.
- [30] C. S. Marchi, B. P. Somerday, S. L. Robinson, *Int. J. Hydrogen Energy* **2007**, *32*, 100.
- [31] A. Drexler, S. He, R. Pippan, L. Romaner, V. I. Razumovskiy, W. Ecker, *Scr. Mater.* **2021**, *194*, 113697.
- [32] A. Drexler, S. He, V. Razumovskiy, L. Romaner, W. Ecker, R. Pippan, *Philos. Mag. Lett.* **2020**, *100*, 513.
- [33] T. T. Fang, M. I. Chen, W. D. Hsu, *AIP Adv.* **2020**, *10*, 065132.
- [34] A. Lob, D. Senk, B. Hallstedt, *Steel Res. Int.* **2011**, *82*, 108.
- [35] A. Michels, W. De Graaff, T. Wassenaar, J. M. H. Levelt, P. Louwerse, *Physica* **1959**, *25*, 25.
- [36] M. Rhode, T. Mente, E. Steppan, J. Steger, T. Kannengiesser, *Weld. World* **2018**, *62*, 277.
- [37] M. Rhode, *Hydrogen Diffusion and Effect on Degradation in Welded Microstructures of Creep-Resistant Low-Alloyed Steels*, BAM, Berlin, Germany **2016**.
- [38] M. Rhode, T. Richter, P. Mayr, A. Nitsche, T. Mente, T. Böllinghaus, *Weld. World* **2020**, *64*, 267.
- [39] A. Drexler, M. Galler, H. Elsayed, R. Vallant, C. Sommitsch, *Int. J. Hydrogen Energy* **2022**, *48*, 7499.
- [40] A. Zafra, Z. Harris, C. Sun, E. Martínez-Pañeda, *J. Nat. Gas Sci. Eng.* **2022**, *98*, 104365.
- [41] A. Drexler, L. Vandewalle, T. Depover, K. Verbeken, J. Domitner, *Int. J. Hydrogen Energy* **2021**, *46*, 39590.
- [42] A. S. Kholobina, R. Pippan, L. Romaner, D. Scheiber, W. Ecker, V. I. Razumovskiy, *Materials* **2020**, *13*, 2288.
- [43] A. Drexler, H. Estilaei, B. Helic, K. Mraczek, in *Proc. of the Steely Hydrogen*, OCAS, Ghent, Belgium **2022**, pp. 1–14.
- [44] A. Drexler, T. Depover, S. Leitner, K. Verbeken, W. Ecker, *J. Alloys Compd.* **2020**, *826*, 154057.
- [45] J. Svoboda, F. D. Fischer, *Acta Mater.* **2012**, *60*, 1211.
- [46] R. A. Oriani, *Acta Metall.* **1970**, *18*, 147.
- [47] H. Shoda, H. Suzuki, K. Takai, Y. Hagihara, *ISIJ Int.* **2010**, *50*, 115.
- [48] A. Drexler, B. Helic, Z. Silvayeh, K. Mraczek, C. Sommitsch, J. Domitner, *J. Mater. Sci.* **2022**, *57*, 4789.
- [49] M. Rhode, T. Schapp, C. Muenster, T. Mente, T. Boellinghaus, T. Kannengiesser, *Weld. World* **2019**, *63*, 511.
- [50] S. Salmi, M. Rhode, S. Jüttner, M. Zinke, *Weld. World* **2015**, *59*, 137.
- [51] M. Truschner, A. Trautmann, G. Mori, *Berg- hüttenmänn. Monatsh* **2021**, *166*, 443.
- [52] J. Venezuela, C. Tapia-Bastidas, Q. Zhou, T. Depover, K. Verbeken, E. Gray, Q. Liu, Q. Liu, M. Zhang, A. Atrens, *Corros. Sci.* **2018**, *132*, 90.
- [53] A. Zafra, L. B. Peral, J. Belzunce, C. Rodríguez, *Int. J. Press. Vessel. Pip.* **2019**, *171*, 34.
- [54] J. A. Nelder, R. Mead, *Comput. J.* **1965**, *7*, 308.
- [55] DIN EN 1594:2013-12 Gas Infrastructure – Pipelines for Maximum Operating Pressure over 16 Bar - Functional Requirements 95.
- [56] C. Wang, J. Zhang, C. Liu, Q. Hu, R. Zhang, X. Xu, H. Yang, Y. Ning, Y. Li, *Int. J. Hydrogen Energy* **2023**, *48*, 243.
- [57] J. P. Hirth, *Metall. Trans. A* **1980**, *11*, 861.
- [58] J. Svoboda, Y. V. Shan, E. Kozeschnik, F. D. Fischer, *Model. Simul. Mater. Sci. Eng.* **2014**, *22*, 065015.
- [59] F. D. Fischer, J. Svoboda, E. Kozeschnik, *Model. Simul. Mater. Sci. Eng.* **2013**, *21*, 025008.
- [60] H. G. Nelson, J. E. Stein, *Gas-Phase Hydrogen Permeation Through Alpha Iron, 4130 Steel, And 304 Stainless Steel From Less than 100 C to Near 600 °C*, NASA, Washington, D.C. **1973**.
- [61] D. Di Stefano, R. Nazarov, T. Hickel, J. Neugebauer, M. Mrovec, C. Elsässer, *Phys. Rev. B* **2016**, *93*, 184108.
- [62] SAE J2579: 2023-01-09, Standard for Fuel Systems in Fuel Cell and Other Hydrogen Vehicles, SAE International, Warrendale, USA **2023**.
- [63] H. Wipf, *Phys. Scr.* **2001**, *T94*, 43.
- [64] H. Wagenblast, H. A. Wriedt, *Metall. Trans.* **1971**, *2*, 1393.
- [65] A. Drexler, B. Helic, Z. Silvayeh, C. Sommitsch, K. Mraczek, J. Domitner, *Key Eng. Mater.* **2022**, *926*, 2077.